Studies of a Nickel-Based Single-Molecule Magnet

Hanspeter Andres,[c] Reto Basler,[c] Alexander J. Blake,[b] Cyril Cadiou,[a] Gregory Chaboussant,[c] Craig M. Grant,[b] Hans-Ulrich Güdel,*[c] Mark Murrie,[c] Simon Parsons,[b] Carley Paulsen,[d]* Fabrizzio Semadini,[f] Vincent Villar,[d] Wolfgang Wernsdorfer,*[e] and Richard E. P. Winpenny*[a]

Abstract: A cyclic complex $[Ni_{12}(chp)_{12}(O_2CMe)_{12}(thf)_6(H_2O)_6]$ (**1**) has been synthesised and studied (chp = 6-chloro-2-pyridonate). Complex **1** exhibits ferromagnetic exchange between the $S=1$ centres, giving an $S=12$ spin ground state. Detailed studies demonstrate that it is a single-molecule magnet with an energy barrier of approximately 10 K for reorientation of magnetisation. Resonant quantum tunnelling is also observed. The field between resonances allows accurate measurement of D, which is 0.067 K. Inelastic neutron scattering studies have allowed exchange parameters to be derived accurately, which was impossible from susceptibility data alone. Three exchange interactions are required: two ferromagnetic nearest neighbour interactions of approximately 11 and 2 cm^{-1} and an anti-ferromagnetic next nearest neighbour interaction of -0.9 cm^{-1}.

Keywords: cage compounds · magnetic properties · neutron diffraction · nickel · single-molecule magnet

Introduction

It is now eight years since it was first observed that a polymetallic cage complex could show hysteresis in a magnetisation versus field plot.[1] This observation, which has led to the neologism "single-molecule magnets" (SMMs) to describe such cages, has attracted enormous interest from both a technological viewpoint—in that such single molecules are the smallest conceivable magnetic memory devices—and from a fundamental scientific perspective, as the cages have allowed studies of quantum mechanical phenomena such as tunnelling.[2]

Since the first reports in this area, based on studies of a $\{Mn_{12}\}$ cluster,[1, 2] several further cages have been shown to behave as SMMs. These include: $\{Fe_8\}$,[3] $\{V_4\}$,[4] $\{Mn_4\}$,[5] $\{Mn_{10}\}$,[6] $\{Fe_4\}$,[7] $\{Fe_{10}\}$[8] and $\{Fe_{19}\}$[9] cages. However the largest energy barrier (E_a) to reorientation of magnetisation remains that reported for the $\{Mn_{12}\}$ cage, with E_a/k of 61 K. Clearly if such cages are ever to have technological application a much higher energy barrier is desirable. As the E_a is related to the spin (S) of the ground state of the cage and the zero-field splitting (D) of that spin, high-spin cages with large magnetic anisotropy are required. The magnetic anisotropy has to be of the Ising-type, that is, the zero-field splitting parameter must be negative to ensure that the $M=\pm S$ states are lowest in energy and the $M=0$ state the highest (for integer spin; for noninteger spin $M=\pm ½$ would be highest). At low temperature only the $M=\pm S$ states are populated; on saturating in a magnetic field only the $M=-S$ level will be populated. When the field is decreased or removed, the return to thermal equilibrium (i.e., equal populations of $M=+S$ and $M=-S$ states) requires the system to "climb the ladder" of M states from $M=-S$ to $M=-S+1$ to $M=-S+2$ and so on to $M=0$, before falling into the second well. This is shown schematically for $S=12$ in Figure 1. The energy barrier is then given by DS^2.

The value of D for the cage can be related, in a first approximation, to the D value of the single ions that form part

[a] Prof. R. E. P. Winpenny, Dr. C. Cadiou
Department of Chemistry, The University of Manchester
Oxford Road, Manchester, M13 9PL (UK).
Fax: (+44) 161-275-4616
E-mail: richard.winpenny@man.ac.uk

[b] Dr. A. J. Blake, Dr. C. M. Grant, Dr. S. Parsons
Department of Chemistry, The University of Edinburgh
West Mains Road, Edinburgh, EH9 3JJ (UK)

[c] Prof. Dr. H.-U. Güdel, Dr. H. Andres, R. Basler,
Dr. G. Chaboussant, Dr. M. Murrie
Department of Chemistry and Biochemistry
University of Bern, Freiestrasse 3
CH-3000 Bern 9 (Switzerland)

[d] Dr. C. Paulsen, V. Villar
CRTBT-CNRS, BP 166, 25 Avenue des Martyrs
38042 Grenoble Cedex 9 (France)

[e] Dr. W. Wernsdorfer
Laboratoire L. Neel-CNRS, BP 166, 25 Avenue des Martyrs
38042 Grenoble Cedex 9 (France)

[f] Dr. F. Semadini
Paul Scherrer Institute
5232 Villigen (Switzerland)

  0947-6539/02/0821-4867 $ 20.00+.50/0

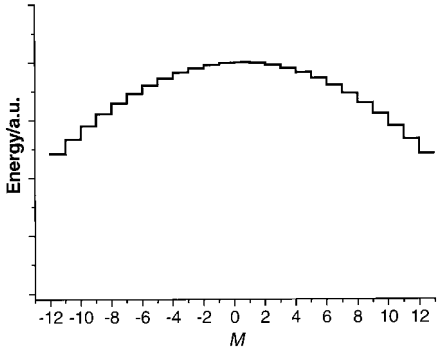

Figure 1. "Ladder" of M states shown schematically for $S = 12$.

of the cage, for example, for $\{Mn_{12}\}$ it can be related to the D value for Mn^{III}.[10] Therefore, ideally a high-spin cage constructed of metal centres that have high D values is required. It has been suggested[11] that Ni^{II}—which often shows ferromagnetic exchange between metals, and is known to have large single-ion zero-field splitting—is an ideal candidate. Here we report detailed investigations of the first nickel-containing SMM. The structure and preliminary magnetic investigations of this molecule were reported several years ago.[12]

Results

Synthesis and structure: Hydrated nickel acetate can be reacted with 6-chloro-2-hydroxypyridine (Hchp) at 130 °C under nitrogen, followed by heating under vacuum to remove the acetic acid byproduct and any unreacted Hchp. Extraction of the resulting green paste with THF gives a green solution, from which green crystals of $[Ni_{12}(chp)_{12}(O_2CMe)_{12}(thf)_6(H_2O)_6]$ (**1**) grow after several days. Crystal data and data collection and refinement parameters are given in Table 1. The molecule structure is shown in Figure 2. The exact procedure followed is given in the Experimental Section; it has been modified from the previously reported synthesis[12] to give a more reliable and better yield, which was necessary to produce sufficient material for inelastic neutron scattering studies.

Table 1. Experimental data for the X-ray diffraction studies of **1**.

	1 · 9 THF
formula	$C_{108}H_{132}Cl_{12}N_{12}Ni_{12}O_{48} \cdot 9\,C_4H_8O$
M_r	4146
crystal system	trigonal
space group	$R\,\bar{3}c$
$a = b$ [Å]	22.764(6)
c [Å]	63.54(3)
V [Å^3]	28516
T [K]	150.0(2)
Z	6[c]
ρ_{calcd} [g cm^{-3}]	1.41
crystal shape and colour	Green block
crystal size [mm]	$0.32 \times 0.32 \times 0.28$
μ [mm^{-1}]	1.41
unique data	2963
unique data with $F_o > 4\sigma(F_o)$	1651
parameters	324
max Δ/σ ratio	0.001
$R1$, $wR2$[a]	0.0737, 0.2534
weighting scheme[b], w^{-1}	$\sigma^2(F_o^2) + (0.1193P)^2$
goodness of fit	1.037
largest residuals [e Å^{-3}]	+0.84/−0.51

[a] $R1$ based on observed data, $wR2$ on all unique data. [b] $P = 1/3[\max(F_o^2, 0) + 2F_c]$. [c] The molecule lies on a $\bar{3}$ axis.

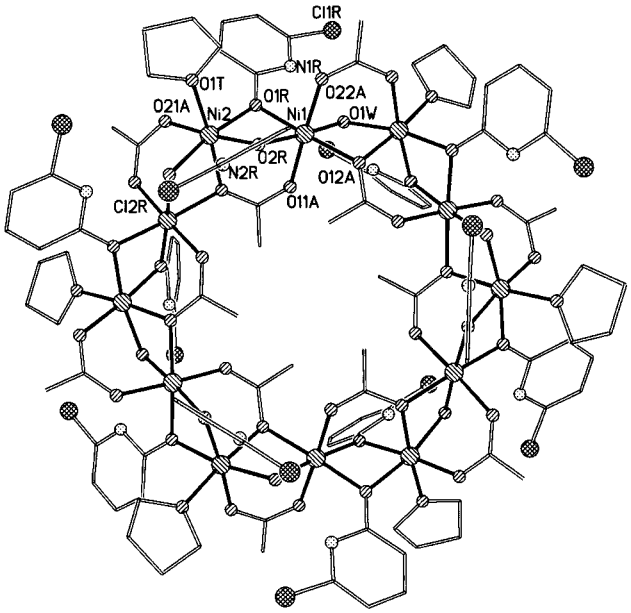

Figure 2. The structure of **1** showing the numbering scheme adopted.

Within the crystal the molecules of **1** are disposed about a crystallographic $\bar{3}$ axis (S_6 symmetry). The result is that there are two independent nickel sites in the asymmetric unit. Both sites are bound to six oxygen atoms; for Ni1 these are derived from one water molecule, three carboxylates and two pyridonates. For Ni2 the oxygen donors come from the bridging water, two carboxylates, two pyridonates and a terminal THF ligand. Both coordination sites have distorted octahedral geometries. Selected bond lengths and angles are given in Table 2.

The two crystallographically independent carboxylate ligands adopt two coordination modes. Outside the metal wheel the carboxylate shows the 2.11 bridging mode (Harris notation[13]), while the carboxylate within the wheel adopts the 3.21 mode. The two chp ligands both adopt the 2.20 mode, binding only through the exocyclic oxygen atom. Therefore, the ring nitrogen donors are not bound to metal centres; however, they are involved in H-bonding interactions with the bridging water molecules. The 2.2 mode adopted by the water molecules is unusual. Ni–O bond lengths show a dependence on the ligand involved; the Ni–O(chp) bonds are all close to 2.04 Å, while those to the bridging water are longer at 2.09 and 2.10 Å as is that to the terminal THF (2.10 Å). The Ni–O(carboxylate) bonds vary between 1.98 and 2.10 Å, with the longer bonds involving the μ_2-oxygen of the 3.21 carboxylate.

The Ni···Ni vectors are therefore bridged in two distinct ways. Ni1···Ni2 is bridged by two oxygen atoms derived from chp ligands, and by the 3.21 carboxylate lying within the wheel. Ni1···Ni2a is bridged by the 2.11 carboxylate outside the wheel, and two μ_2-oxygen atoms derived from a water and

0947-6539/02/0821-4868 $ 20.00+.50/0 Chem. Eur. J. 2002, 8, No. 21

Table 2. Selected bond lengths [Å] and angles [°] for **1**.

Ni1−O22A#1	2.012(10)
Ni1−NI2#1	3.106(3)
Ni1−O11A#2	2.013(9)
Ni2−O21A	1.977(9)
Ni1−O1R	2.038(9)
Ni2−O2R	2.037(10)
Ni1−O2R	2.045(10)
Ni2−O1R	2.045(9)
Ni1−O1W	2.087(9)
Ni2−O12A#2	2.067(9)
Ni1−O12A	2.103(9)
Ni2−O1T	2.100(9)
Ni1−NI2	3.066(3)
Ni2−O1W#2	2.102(9)
O22A#1-Ni1-O11A#2	177.4(4)
O21A-Ni2-O2R	175.1(4)
O22A#1-Ni1-O1R	89.7(4)
O21A-Ni2-O1R	97.8(4)
O11A#2-Ni1-O1R	91.4(4)
O2R-Ni2-O1R	78.9(4)
O22A#1-Ni1-O2R	92.4(4)
O21A-Ni2-O12A#2	92.7(4)
O11A#2-Ni1-O2R	90.1(4)
O2R-Ni2-O12A#2	91.1(4)
O1R-Ni1-O2R	78.8(4)
O1R-Ni2-O12A#2	93.8(4)
O22A#1-Ni1-O1W	89.3(4)
O21A-Ni2-O1T	87.3(4)
O11A#2-Ni1-O1W	88.3(4)
O2R-Ni2-O1T	89.3(4)
O1R-Ni1-O1W	94.6(3)
O1R-Ni2-O1T	92.6(4)
O2R-Ni1-O1W	173.2(4)
O12A#2-Ni2-O1T	173.6(4)
O22A#1-Ni1-O12A	90.4(4)
O21A-Ni2-O1W#2	91.7(4)
O11A#2-Ni1-O12A	88.3(4)
O2R-Ni2-O1W#2	92.0(4)
O1R-Ni1-O12A	174.6(4)
O1R-Ni2-O1W#2	169.2(4)
O2R-Ni1-O12A	106.5(4)
O12A#2-Ni2-O1W#2	80.5(4)
O1W-Ni1-O12A	80.0(3)
O1T-Ni2-O1W#2	93.1(4)

the 3.21 acetate. These chemically distinct bridges lead to distinct super-exchange paths, which influence the magnetic properties of **1** (see below).

Complex **1** crystallises in the rhombohedral space group $R\bar{3}c$. Within the crystal all the molecules of **1** pack parallel to one another and normal to the c axis (Figure 3). This is an important advantage when single-crystal magnetic studies are performed (see below). The centroid···centroid distance between rings is 16.9 Å, while the nearest inter-ring Ni···Ni contact is 10.7 Å.

With other mixtures of pyridonates and carboxylates, and for solvents such as MeCN or CH_2Cl_2, cages of nuclearity ten to twelve form from this reaction with structures related to centred, pentacapped trigonal prisms.[14] For example, a dodecanuclear cage with the formula $[Ni_{12}(OH)_6(mhp)_{12}(O_2CCH_2Cl)_6]$ (**2**; mhp = 6-methyl-2-pyridonate) has been structurally characterised. Our initial thoughts were that the differences in structure between **1** and **2** were due to the pyridonate ligand present. In chp the presence of the electron-withdrawing chlorine group in the 6-position of the ring reduces the basicity of the ring nitrogen atom, and, hence, allows formation of a structure in which the N atom does not bind. This stabilises the 2.20 binding mode. For mhp, the electron-releasing methyl group pushes into the ring, increasing the basicity of the ring nitrogen atom and, hence, the N atom is always found bound to a metal, and the 2.11 and 3.21 binding modes are favoured with the 2.20 mode excluded.

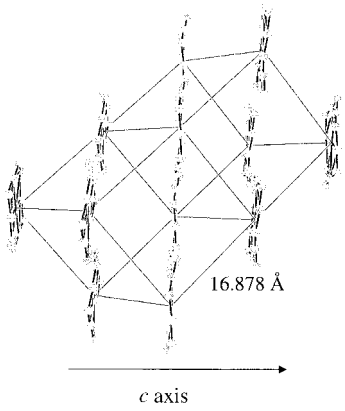

Figure 3. The packing of **1** in the crystal.

However we noticed that samples of **1** that had been kept for several months began to smell of vinegar; this suggests the formation of acetic acid. To investigate this decomposition process further we performed thermogravimetric analysis on fresh crystals of **1**, heating at a rate of 5° per minute (Figure 4).

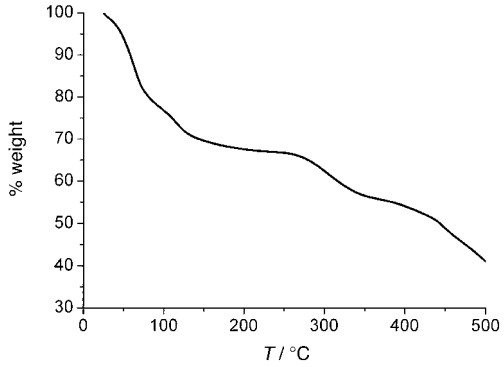

Figure 4. Thermogravimetric data for **1**.

We observed three distinct weight losses up to 260 °C. The first, up to around 74 °C, is a loss of around 18 % of the weight of the crystals; this is greater than the loss of nine molecules of lattice THF alone. Up to 130 °C 29 % of the mass is lost, which is greater than the loss of the nine lattice and six bound THF molecules. Up to 260 °C the mass lost is 33.1 %. This matches almost perfectly with nine lattice and six bound THF molecules and six molecules of acetic acid (calculated mass loss 33.6 %). Assuming this is the case then we can write the following equation for the decomposition of **1** [Eq. (1)]:

$$[Ni_{12}(chp)_{12}(O_2CMe)_{12}(thf)_6(H_2O)_6].9\,THF \rightarrow 15\,THF + 6\,HO_2CMe + \mathbf{A} \quad (1)$$

If **A** is a single chemical species it has the formula: $[Ni_{12}(OH)_6(chp)_{12}(O_2CMe)_6]$. This is analogous to the formula

of the centred, pentacapped trigonal prism **2**. Therefore it is possible that the cyclic dodecanuclear species **1** is an intermediate on the way towards formation of a trigonal prismatic structure. Attempts to recrystallise **A** from non-coordinating solvents have thus far failed. Recrystallisation of **A** from MeOH gives a known trinuclear complex $[Ni_3(chp)_2(O_2CMe)_4(MeOH)_6]$ in low yield.[15] X-ray powder diffraction studies of **A** show it to be an amorphous material.

Magnetic studies: In the preliminary communication concerning **1** initial magnetic studies were reported that suggested that **1** has an $S=12$ ground state due to ferromagnetic exchange between the Ni^{II} centres. Here we report low-temperature studies that confirm this high-spin ground state, and that demonstrate **1** is a single-molecule magnet.

An isothermal magnetisation study at 150 mK shows unequivocally that the molecule has an $S=12$ ground state (Figure 5). The saturation value of 25.5 μ_B gives a g value of

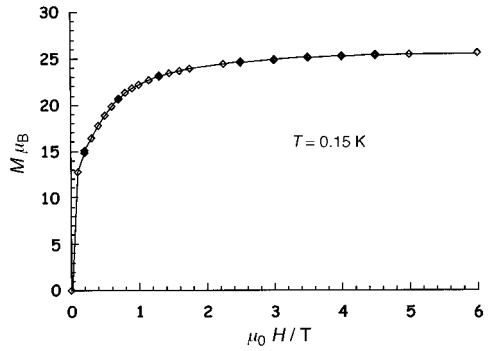

Figure 5. Magnetisation of a powder sample of **1** at 150 mK.

2.13. A more unexpected observation is that in a plot of $1/\chi'$ against temperature (whereby χ' is the in-phase magnetic susceptibility), that is, a traditional Curie–Weiss plot, data below 1.2 K lie on a straight line, and that this line has a positive intercept at 250 mK (Figure 6). This indicates ferromagnetic exchange; however, as the vast majority of molecules are already in the spin ground state at 1.2 K this exchange must be *between* $S=12$ molecules rather than within the nickel wheels. This intermolecular interaction is unexpected, and difficult to explain (see the Discussion section below).

Studies of the susceptibility behaviour of powdered samples of **1** in an alternating external field show the frequency-dependent maximum in the out-of-phase susceptibility (χ'') typical of a single-molecule magnet (Figure 7). This data can be analysed by using an Arrhenius treatment as the frequency (υ) at which the external field is varied is related to the relaxation time τ at the temperature at which χ'' is a maximum. The relationship is given by Equation (2).

$$\tau = 1/2\pi\upsilon \qquad (2)$$

Therefore in a plot of $\ln\tau$ against $1/T$, the activation energy is the slope. This treatment gives an energy barrier for reorientation of magnetisation (E_a/k) of between 9 and 10 K for **1** (Figure 8). The exact value is not certain as at very low

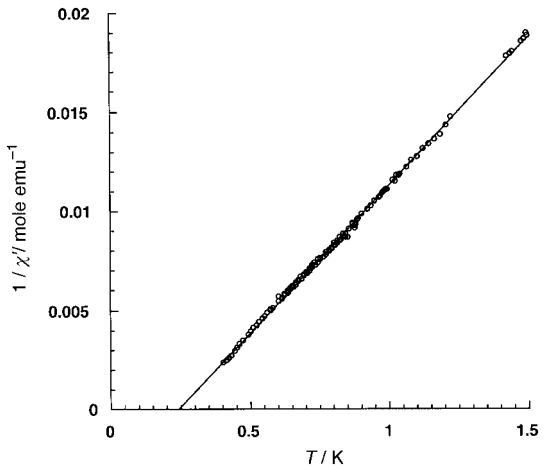

Figure 6. $1/\chi'$ against T for a powder sample of **1** from 0.4 to 1.2 K, showing the positive Weiss constant.

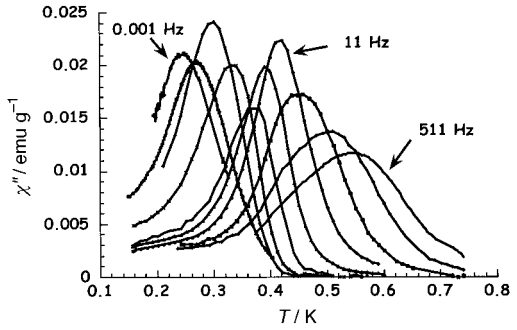

Figure 7. χ'' against T for a powder sample of **1**. The figure shows ten different frequencies, with peaks from left to right for 0.001, 0.003, 0.011, 0.057, 0.57, 2.11, 11.1, 57, 211 and 511 Hz.

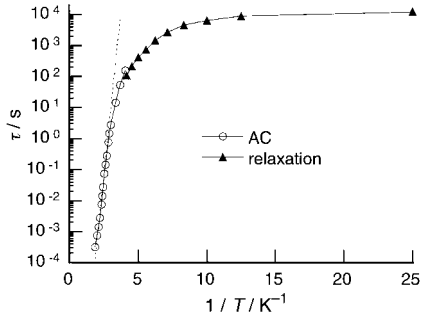

Figure 8. τ against $1/T$ for **1**.

temperature it appears that the relaxation rate is no longer following a simple Arrhenius law as non-thermal relaxation routes, that is, tunnelling (see below) becomes important. This value of E_a/k allows us to estimate D/k as being between 0.063 and 0.069 K. Measurements of relaxation times on single crystals of **1** at even lower temperatures show the relaxation rate becoming temperature independent. Combining the data from AC susceptibility and relaxation measurements clearly shows that below approximately 0.2 K a nonthermal relaxation path is operative and the Arrhenius law no longer applies (Figure 8).

Measurements on single crystals of **1**, orientated so that the field is parallel to the crystallographic c axis, show hysteresis in plots of magnetisation against field. For example, at sweep

0947-6539/02/0821-4870 $ 20.00+.50/0 *Chem. Eur. J.* **2002**, *8*, No. 21

rates of 35 mT s^{-1} hysteresis is clearly seen below 400 mK (Figure 9), and at 250 mK and lower temperatures "steps" are resolved on this loop, indicative of quantum tunnelling of magnetisation. These steps are best resolved below 100 mK, and can be seen at 0 and ± 0.047 T, and less clearly at ± 0.094 T, and are due to sudden loss of magnetisation as $-M$ levels within the $S = 12$ spin ground state manifold come into

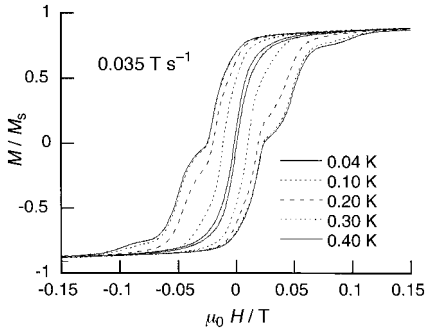

Figure 9. Magnetisation against field for a single crystal of **1**, measured parallel to the *c* axis at 0.035 T s^{-1}, varying the temperature.

resonance with $+M$ levels on the other side of the energy barrier; this allows tunnelling of the magnetisation through this barrier. The levels cross when $H = nD/g\mu_B$ (where n = an integer). Here the field between two resonances is 0.047 T and $g = 2.13$, therefore we can calculate $D/k = 0.067$ K which is in very good agreement to the value calculated from measurements of out-of-phase susceptibility. The energy barrier would then be 9.6 K.

As tunnelling depends on energy levels on either side of the barrier being in resonance, it is dependent on the sweep rate of the experiment. At slow sweep rates the $M = \pm 12$ levels for **1** remain degenerate for sufficient time that most of the magnetisation tunnels through the barrier at $H = 0$ (Figure 10). At faster sweep rates, for example, 17 and 35 mT s^{-1} there is insufficient time for all tunnelling to take place at $H = 0$, and, therefore, a step becomes resolved before the second

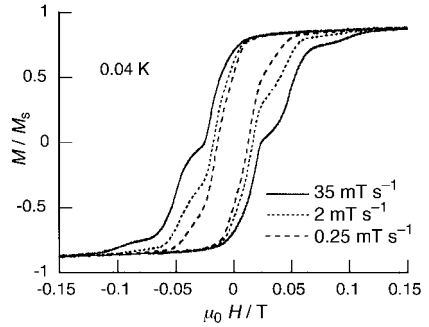

Figure 10. Magnetisation against field for a single crystal of **1**, measured parallel to the *c* axis at 0.04 K, varying the rate of change of field.

tunnelling event at ± 0.047 T. The tunnelling can also be influenced by the presence of a transverse magnetic field, that is, perpendicular to the easy axis of magnetisation. This is shown in Figure 11; in a zero transverse field two tunnelling steps are clearly seen, while for transverse fields of 0.168 T and

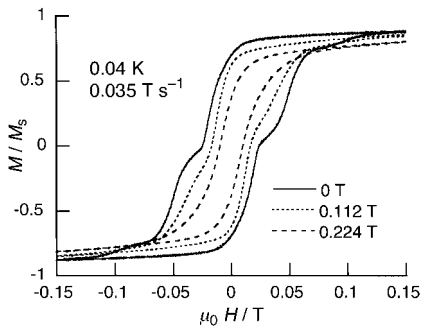

Figure 11. Magnetisation against field for a single crystal of **1**, measured parallel to the *c* axis at 0.04 K and 0.035 T s^{-1}, varying the transverse magnetic field.

greater the tunnelling at about 0 T is so large no further steps are seen as all magnetisation has been lost.

To complete the study of the quantum tunnelling, minor cycles experiments were carried out (Figure 12). After saturation at -0.15 T, the field is swept towards different positive values and then reversed. When the field is reversed

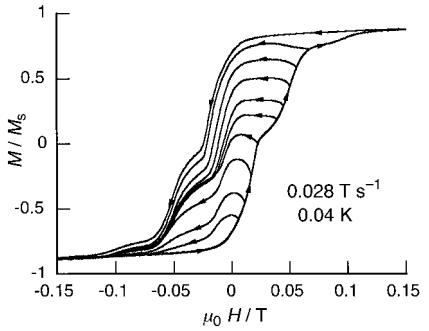

Figure 12. Minor cycle experiments on **1** at recorded at 0.04 K and 0.028 T s^{-1} sweep rates.

during the first tunnelling step, the tunnelling from $M = -12$ to $M = +12$ energy levels continues until zero field is reached; then it is possible to see at zero field the step corresponding to the $M = +12$ to $M = -12$ transition and at -0.047 T the second step ($M = +12$ to $M = -11$). When the field is reversed during the second quantum step, the excited level $M = +11$ becomes populated and relaxes immediately to $M = +12$ with a phonon emission and then at zero field the same process than the one previously described is followed.

Inelastic neutron scattering (INS): Figure 13a shows an overview INS spectrum at $T = 1.6$ K and in Figure 13b the region of excitations is shown for several values of the scattering vector Q. At $T = 1.6$ K, the instrumental resolution at the elastic peak position is 64 μeV and increases with increasing energy transfer to 170–190 μeV between 2.8 and 3.4 meV. In the range 0–3.8 meV only two broad inelastic peaks can be observed for all Q values. These spectra are best reproduced with a linear background and two Gaussians centered at 2.85(1) and 3.35(1) meV. These transitions are labeled I and II, respectively. Their Q dependence, extracted from the fitting procedure, is shown in Figure 14a. For both transitions the Q

  0947-6539/02/0821-4871 $ 20.00+.50/0

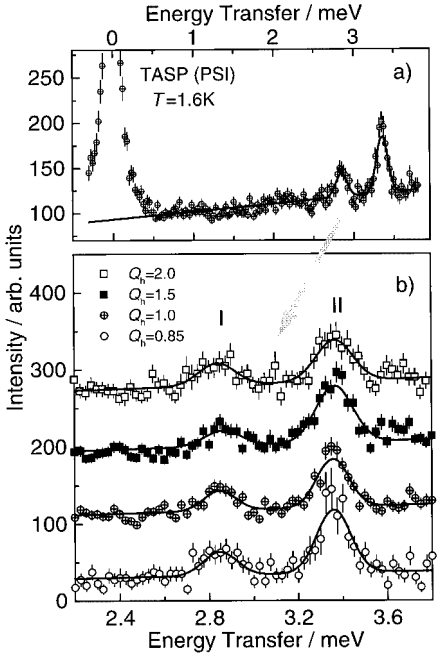

Figure 13. Inelastic neutron scattering spectra of **1** at $T = 1.5$ K for various values of Q. The least squares Gaussians fits are shown as solid lines. The two transitions are labelled I and II.

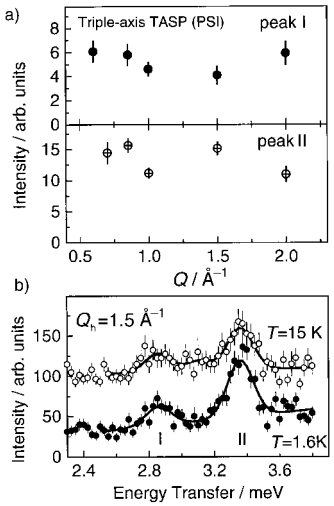

Figure 14. a) Q dependence of the two inelastic transitions I and II shown in Figure-13; b) transitions I and II at two different temperatures.

dependence is very weak and almost flat. This is an artefact due to the large amount of hydrogen in the sample, which is responsible for the loss of Q resolution: multiple incoherent scattering on the H nuclei leads to loss of Q resolution and thus a blurring of Q dependent features.

To identify the nature of these transitions (magnetic or phonon scattering) it is therefore necessary to look at their temperature dependence as well. Figure 14b shows two spectra at $T = 1.6$ K and $T = 15$ K for $Q = 1.5$ Å^{-1}. Both transitions weaken and broaden slightly as the temperature is increased. Phonon modes increase with temperature and their intensities increase as Q^2.[16] We conclude that the two peaks at 2.85 and 3.35 meV are due to magnetic excitations. As these peaks are observed at both 1.6 and 15 K they originate in the $S = 12$ ground state and are presumably transitions between the $S = 12$ state and the first excited states, that is, the $S = 11$ states. The detailed interpretation of these results is complicated, and is discussed below.

Discussion

Structural and synthetic studies: Compound **1** belongs to a family of cages that result from reaction of cobalt or nickel salts with a blend of carboxylates and pyridonates. The other members of the family appear to have radically different structures. Most are based on centred, pentacapped trigonal prisms, or fragments thereof.[14, 18] We have shown that all these cages can be related to the structure of the mineral $Ni(OH)_2$, which is a layered-structure related to the cadmium iodide structure.[17] The metal vertices of **1** can be recognised in the mineral.

It is briefly worth speculating as to why the cyclic structures form for **1**, rather than the more compact cages generally found for these reactions involving metal/carboxylate/pyridonate. The wheels only form when the pyridonate features an electron-withdrawing substituent in the 6-position, when the carboxylate is acetate and when the solvent is THF. The electron-withdrawing substituent of the pyridonate allows the 2.20-binding mode to occur, which is vital for the formation of the wheel. The choice of carboxylate is restricted to acetate, presumably because the methyl groups of the acetate ligands fit together well at the centre of the metallocycle; larger carboxylates would not fit into this cavity. This suggests an experiment with larger carboxylates that might lead to larger wheels with more capacious cavities, but unfortunately this experiment does not work. Surprisingly it has not yet been possible to crystallise derivatives with other solvents in place of THF in the sixth position of the second nickel site in the structure.

The thermogravimetric analysis suggests that **1** may be an intermediate on the way towards the centred, pentacapped trigonal prisms. We have observed a somewhat similar reactivity for chromium(III) benzoate clusters.[18] Heating $[Cr_3O(O_2CPh)_6(OH)(H_2O)_2]$ to above 300 °C causes dehydration and gives an octanuclear cage $[Cr_8O_4(O_2CPh)_{16}]$ with a structure of approximately T_d symmetry, involving a central Cr_4O_4 heterocubane with an additional Cr atom attached to each oxide centre.[18] At lower temperatures, approximately 200 °C, we can isolate a cyclic octanuclear cage $[\{Cr(OH)(O_2CPh)_2\}_8]$ albeit in low yield. Mass balance would suggest that the Cr_8 wheel involves less loss of water from the initial triangle than for the Cr_8 cage; therefore it may be an intermediate. In the nickel chemistry the transformation of **1** into the trigonal prismatic structures would be a desolvation and decarboxylation, while the transformation in the chromium chemistry involves loss of solvent (water) only. The hypothesis that firstly wheels form and then condense further into compact cages is unproven but intriguing. It suggests several new synthetic routes to pursue, either to trap cyclic "intermediates", or to decompose wheels into new compact cages by application of more rigorous conditions.

Exchange integrals and inelastic neutron scattering: The $S = 12$ ground state of **1** is due to ferromagnetic exchange between

  0947-6539/02/0821-4872 $ 20.00+.50/0 *Chem. Eur. J.* **2002**, *8*, No. 21

the nickel centres. The magnitude of this exchange is not easily determined; however, use of quantum statistical mechanics[19] has allowed the temperature-dependent susceptibility behaviour to be modelled from 1.8 to 300 K by assuming a single exchange integral, $J = 6\ \mathrm{cm}^{-1}$ and $g = 2.23$. It is immediately apparent that the calculated g value differs from the measured g value at 150 mK (see above).

Magnetic INS is a powerful tool to obtain an intimate insight into the exchange couplings that are responsible for the magnetic properties of molecular magnets.[20] An incoming neutron $(E_i,\boldsymbol{k}_i)$ exchanges energy and wave vector with the spin system in the sample through the electromagnetic interaction between the neutron's spin and the system's spin. The scattered neutron $(E_f,\boldsymbol{k}_f)$ is detected after the scattering process. The conservation laws impose that the spin system experiences an energy change $\hbar\omega = E_i - E_f$ and a momentum transfer $Q = \boldsymbol{k}_i - \boldsymbol{k}_f$. One important consequence is that only transitions between spin states that fulfil well-defined selection rules will have a nonzero intensity. If $E(S,M)$ and $E(S',M')$ are the initial and final states in the neutron scattering event, repectively, possible INS transitions are governed by the following selection rules: $\Delta S = S - S' = 0,\ \pm 1;\ \Delta M = M - M' = 0, \pm 1$.

Assuming that at low enough temperatures only the ground state is thermally populated, it is possible to directly assign a given INS peak to a transition from the ground state to higher excited states. The observation of those transitions allows a detailed determination of the energy levels from which the exchange couplings are derived.

In the dipole approximation, the neutron scattering cross section is proportional to the magnetic scattering function $S(Q,\omega)$ [Eq. (3)]:[21]

$$S(Q,\omega) \approx N[f(Q)]^2 \sum_{if} p_i |\langle f|S_\perp|i\rangle|^2 \delta(\hbar\omega - [E_f - E_i]) \qquad (3)$$

in which N is the number of magnetic centers in the sample, $f(Q)$ is the magnetic form factor, $\hbar\omega$ is the neutron energy transfer, E_i and E_f are the neutron initial and final energy, respectively, and p_i is the Boltzmann factor for initial state $|i\rangle$. The total neutron scattering cross section is obtained by summing up all the possible initial and final states.

Firstly, in order to analyse the data, we need to consider the possible exchange couplings that are relevant in this system. Figure 2 shows **1** viewed along the c axis. There are two inequivalent Ni^{II} sites with approximate NiO_6 octahedral local symmetry. Figure 15a shows the relevant part of the wheel. We see immediately that there are two different exchange pathways between nearest neighbour Ni^{II} ions: one involves two μ_2-oxygen bridges and an inner 3.21-acetate bridge, and a second involves two μ_2-oxygen bridges and an outer 2.11-acetate bridge. There is also a pathway through the inner carboxylate groups between next-nearest Ni1 neighbours.

So to account for this, we should model the exchange coupling in **1** by using the three exchange parameters J_1, J_2 and J_3 as indicated in Figure 15b. The Hamiltonian is then given by Equation (4):

$$H = -J_1 \sum_i S_i S_{i+1} - J_2 \sum_i S_{i+1} S_{i+2} - J_3 \sum_i S_i S_{i+2} \qquad (4)$$

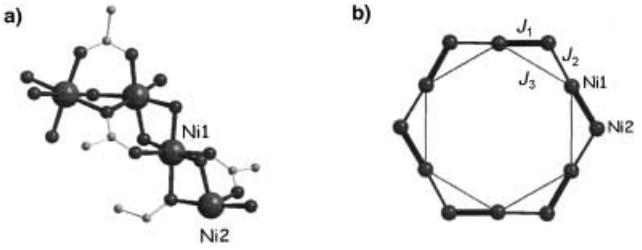

Figure 15. a) Close up look at the exchange pathways corresponding to J_1, J_2 and J_3; b) schematic representation of the exchange couplings between the Ni^{II} $S = 1$ ions.

(The convention adopted has $J > 0$ for ferromagnetic exchange, with $i = 1, 2,.., N-2$, whereby $N = 12$ and $i + 12 = i$)

In the previously published analysis of the magnetic susceptibility J_3 was neglected and $J_1 = J_2$ was assumed.[19] The experimental χT versus T curve was well reproduced with this model and a J_1 value of $6-6.8\ \mathrm{cm}^{-1}$ was derived.[19]

The power of INS is that the cluster energy levels are directly determined. INS unambiguously settles the question whether a model with equal or with alternating nearest-neighbour interactions is the correct one. We calculated the eigenvalues of Equation (3) by using the program MAGPACK[22] for the following two cases: a) $J_1 = J_2$, $J_3 = 0$ and b) $J_1 > J_2$, $J_3 = 0$ (the same result would be obtained for $J_2 > J_1$). The result is shown in Figure 16. In both cases $S = 12$ is the

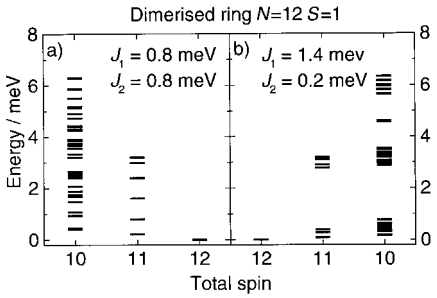

Figure 16. Calculated energy levels ($S \geq 10$ only) for a wheel with 12 spins $S = 1$ a) for the uniform model ($J_1 = J_2$) and b) the strongly dimerised limit ($J_1 \gg J_2$). The sum ($J_1 + J_2$) is constant for both cases.

cluster ground state for a ferromagnetic J_1. In the uniform model (Figure 16, left-hand side) there are seven levels within the first 4 meV. With the selection rules $\Delta S = 0, \pm 1$, all are accessible by INS from the $S = 12$ ground state. In the model with alternate coupling, the energy pattern looks very different (see Figure 16, right-hand side). The seven levels are bunched in two groups, one consisting of three levels within 0.5 meV from the $S = 12$ and the other ones around 3 meV. From our INS spectrum (Figure 13) we see that there are no magnetic transitions between 0.5 and 2.83 meV. This immediately tells us that the model with equal interactions between the nearest neighbours is not correct. We therefore systematically varied the J_1/J_2 ratio. The result is shown in Figure 17. A strong dimerisation is needed to account for the experimental data. The $J_1 = 1.4$ and $J_2 = 0.2$ meV values used for the calculation could explain the 2.85 and 3.35 meV peaks.

  0947-6539/02/0821-4873 $ 20.00+.50/0

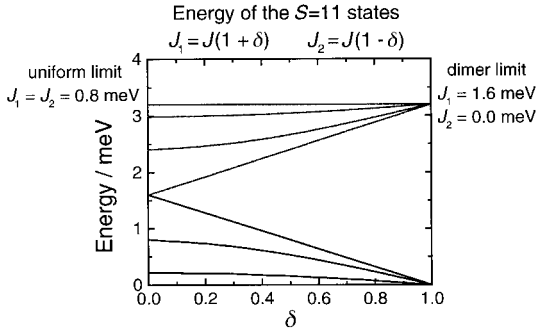

Figure 17. Calculated energy levels of the $S=11$ states as a function of J_1 and J_2 ($J_3=0$). The $S=12$ ground state is set to zero. In the uniform limit, the energy levels are evenly distributed between 0 and 3.2 meV $=4J_1$. In the dimer limit ($J_2=0$), all levels collapse either towards $E=0$ or $E=2J_1$ as expected for a set of isolated $S=2$ dimers.

However, in this scenario, one expects also INS peaks arising from transitions to the lower $S=11$ levels at positions up to 0.5 meV. This is clearly ruled out by the experiment. Figure 13 shows that no such INS peaks exist.

To correct this we introduce the next nearest neighbour interaction J_3. Figure 18 shows the $S=11$ levels as a function of J_3 for $J_1=1.4$ and $J_2=0.2$ meV. When J_3 is ferromagnetic

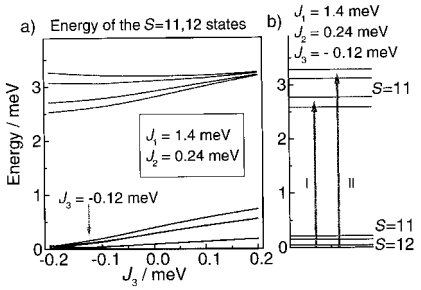

Figure 18. a) Calculated energy levels of the $S=11$ and the $S=12$ states as a function of J_3. For positive J_3 (FM) the upper $S=11$ levels merge into almost a single level while the lower $S=11$ levels spread further. For negative J_3 (AFM) the trend is reversed with the upper $S=11$ levels forming a double set of levels and the lower $S=11$ levels merging to even lower energies. b) Energy level diagram for $J_1=1.40$, $J_2=0.24$ and $J_3=0.12$ meV. The two arrows represent the observed INS transitions.

(positive) the upper $S=11$ levels merge into almost a single level, while the lower $S=11$ levels extend in energy. For antiferromagnetic J_3 (negative) the trend is reversed, with the upper $S=11$ levels mildly affected but the lower $S=11$ level splitting decreasing. At some critical value $J_3 \geq -J_2$, the $S=12$ level is no longer the ground state.

Intuitively, this competition between J_2 and J_3, if J_3 is negative, determines whether the strongly ferromagnetically bound $S=2$ dimers order ferro- or antiferromagnetically along the wheel. For $|J_3|>|J_2|$ we should get an $S=0$ cluster ground state. In **1**, the ground state is $S=12$, and from an analysis of our experimental data we get: $J_1 \sim 1.40(5)$ meV $=$ 11.3(4) cm^{-1}, $J_2 \sim 0.24(3)$ meV $= 1.9(2)$ cm^{-1} and $J_3 \sim -0.12(2)$ meV $= -0.9(1)$ cm^{-1}.

The observation of three exchange interactions reflects the presence of three chemically distinct super-exchange paths in the structure. They differ both chemically, in the nature of the two μ_2-oxygen atoms involved, and metrically, as the Ni–O bond distances and Ni-O-Ni angles also vary (see Table 2). For one exchange path, the Ni_2O_2 rings feature two oxygen atoms from chp ligands, and the Ni-O-Ni angles are both 97.4(4)°; in the second ring the O atoms come from a water molecule and from an acetate ligand and the two Ni-O-Ni angles are 95.7(4) and 96.3(4)°, respectively. Given the magneto-structural correlations for Ni clusters published by the groups of Thompson[23] and Christou,[24] both of which relate the exchange interaction to the angle at bridging O atoms, it is entirely reasonable to expect there to be two exchange integrals, that is, $J_1 \neq J_2$, for the nearest neighbour interaction. If the angle is the more important factor then the Ni···Ni interaction bridged by water and acetate should be the more ferromagnetic, that is, J_1. However the chemical species involved in each bridge are different, and this conclusion is debatable. Others may argue that a bridging water molecule is a poor communicator of magnetic information, and, therefore, the bridge involving this molecule should be the less ferromagnetic.

The involvement of a next nearest neighbour interaction, J_3, through the carboxylate ligand acting in a *syn-anti*-bridging mode, is not unprecedented.

Intermolecular exchange interactions: The observation of a positive Weiss constant ($\theta_{cw}=+0.25$ K, see Figure 6) for the low-temperature susceptibility measurements was unexpected, implying a ferromagnetic intermolecular interaction. Ideally the constant should be derived from data measured well above the Weiss constant; however, here where intermolecular interactions between $S=12$ ground states are being studied, this is impossible as excited states become occupied at higher temperatures.

The separation of the molecules and the absence of an evident super-exchange path between the molecules in the crystals suggest—at least initially—that this intermolecular interaction could be dipolar in nature. We have therefore estimated the magnitude of the dipolar interaction using two approximations. Note that these calculations give a size for this interaction, but would normally give an antiferromagnetic intermolecular exchange.

Firstly use of equations used in EPR spectroscopy to calculate dipole–dipole interactions between point magnetic dipoles,[25] gives a value of 0.22 K for the interaction between two $S=12$ centres separated by 16.7 Å. Use of the mean-field approximation[26] gives a lower value of 0.08 K. The observed intercept of 0.25 K is therefore of the same order of magnitude as these two calculated values. However, while the magnitude is approximately correct it is inexplicable that this intermolecular dipolar interaction is ferromagnetic.

A ferromagnetic exchange would be more explicable if super-exchange were operational. The only protic H atoms in the structure, which are attached to the bridging water molecules, are involved in intermolecular hydrogen bonds, and there is little evidence for interactions through aromatic systems of the pyridonate ligands. However the shortest intermolecular contacts are between a Cl atom of a chp ligand in one wheel and a hydrogen atom in the aromatic system of a pyridonate ligand in a neighbouring wheel. The Cl···H–C

  0947-6539/02/0821-4874 $ 20.00+.50/0 *Chem. Eur. J.* **2002**, *8*, No. 21

contact is 3.62 Å. A similar H-bonding interaction between a pair of $\{Mn_4\}$ cages has been shown to lead to exchange-biasing of quantum tunnelling.[27] Therefore it seems possible this very weak H-bonding interaction is acting as a super-exchange path, and thus influences the magnetic behaviour of **1** at very low temperatures. It is clear that in order to understand measurements made at very low temperatures even apparently negligible intermolecular interaction paths must be carefully considered.

Near 400 mK the magnitude of the susceptibility is very close to what one would expect for a ferromagnetic transition; when corrections are made the susceptibility has a value close to $1/N$, whereby N is the demagnetisation coefficient. The close proximity to a phase transition may also explain the anomalous intensities of the frequency dependent out-of-phase susceptibility peaks, that is, they pass through a minimum at 350 mK. It may be that tunnelling of the magnetisation within the clusters is competing with the formation of an ordered ferromagnetic state. Similar features have been observed in the single-molecule magnet $\{Fe_8\}$.[28] Further studies will be required to answer these questions definitively.

Tunnelling: Quantum tunnelling of magnetisation has been observed in five previous families of SMMs: $\{Mn_{12}\}$ cages with $S = 19/2$ and 10 ground states,[2] $\{Mn_4\}$ cages with $S = 9/2$ and 8,[5] $\{Mn_9\}$ cages with $S = 11/2$; $\{Fe_8\}$ cages with $S = 10$[3] and an $\{Fe_4\}$ cage with $S = 5$.[7] Complex **1** is therefore the highest spin cage to show tunnelling, and the first example with nickel. While higher spin SMMs are known, for example, the $\{Fe_{19}\}$ cages reported by Heath et al,[9] in these examples tunnelling appears to be quenched by intermolecular exchange. Here tunnelling is observed despite significant intermolecular interactions. It is also surprising tunnelling is observed while the magnetic anisotropy is so low.

Conclusion

These results extend the range of SMMs known, both by including a new metal as the spin centre, but also by being the highest spin molecule to show quantum tunnelling of magnetisation.

The results from inelastic neutron scattering (INS) demonstrate the strength of this technique as a method for determining exchange interactions. In this case a previously published analysis[19] of the exchange interactions adequately models the magnetic susceptibility data, but does not model the INS data at all. If accurate magneto-structural correlations are to be developed it is vital that the magnetic parameters are precisely measured; for clusters as complex as **1** susceptibility data alone is no longer sufficient.

Experimental Section

Preparation of compounds: All reagents, metal salts and ligands were used as obtained from Aldrich. Analytical data were obtained on a Perkin–Elmer 2400 Elemental Analyser by the University of Edinburgh Microanalytical Service.

$[Ni_{12}(chp)_{12}(O_2CMe)_{12}(thf)_6(H_2O)_6]$ (1): Hydrated nickel acetate (2.51 g, 10.1 mmol) was ground together with Hchp (2.77 g, 21.4 mmol). The light green powder was then transferred to a Schlenk tube and purged with N_2 for 15 mins. The mixture was heated to 130 °C under N_2 to form a clear green melt. After approximately 30 mins, acetic acid that had formed during the reaction was removed under reduced pressure. Then excess Hchp was removed by sublimation to leave a bright green solid (2.70 g). THF (30 mL) was added to the solid, and the mixture stirred at ambient temperature. After filtration through first paper then celite, the bright green solution was divided into four portions, and placed in vials that were closed. After 2–3 days the green crystals that had formed in the vials were collected by filtration and washed with ice-cold THF. Yield: 50 % 1.5 g; elemental analysis calcd (%) for $C_{108}H_{132}Cl_{12}N_{12}Ni_{12}O_{48}$(4146): C 37.1, H 3.8, N 4.8; found: C 36.9, H 3.7, N 5.1.

Crystallography: Crystal data and data collection and refinement parameters for compound **1** are given in Table 1, selected bond lengths and angles in Table 2.

Data collection and processing: Data for **1** were collected on a Stoë Stadi-4 four-circle diffractometer equipped with an Oxford Cryosystems low-temperature device,[29] graphite-monochromated $Mo_{K\alpha}$ radiation ω-scans and the learnt-profile method.[30] Data were corrected for Lorentz and polarisation factors.

Structure analysis and refinement: Structure **1** was solved by the heavy atom method by using DIRDIF.[31] Both structures were completed by iterative cycles of ΔF syntheses and full-matrix least-squares refinement. All full-weight non-H atoms were refined anisotropically. The bound THF molecule showed disorder, which was modelled with eight half-weight C atoms. The disordered solvent molecules in all structures were refined isotropically. In both structures full-weight H atoms attached to C atoms were included in idealised positions, allowed to ride on their parent C atoms (C–H 0.96 Å), and assigned isotropic thermal parameters [$U(H) = 1.2\ U_{eq}(C)$]. Full-weight H atoms attached to O atoms were included in positions to maximise H-bonding interactions, and assigned isotropic thermal parameters [$U(H) = 1.5\ U_{eq}(O)$]. Partial weight H atoms were not included in refinements. All refinements were against F^2 and used SHELXL-93.[32]

CCDC-187924 contains the supplementary crystallographic data for the structure reported in this paper. These data can be obtained free of charge via www.ccdc.cam.ac.uk/conts/retrieving.html (or from the Cambridge Crystallographic Data Centre, 12 Union Road, Cambridge CB2 1EZ, UK; fax: (+44) 1223 336–033; or e-mail: deposit@ccdc.cam.ac.uk).

Magnetic measurements: Ac susceptibility and dc magnetization measurements were performed with the high-field low-temperature SQUID magnetometer developed at the CRTBT. Approximately 1 mg of powder sample was mixed with some vacuum grease and attached to a long copper coil foil sample holder, which in turn was thermally anchored to the bottom of a mixing chamber of a miniature dilution refrigerator. The sample holder assembly was isolated from the He bath by a quartz vacuum chamber, and descended into the bore of an 8 tesla superconducting magnet. Absolute value measurements of the susceptibility and magnetization were made by extracting the sample through the gradiometer detection coils. The very low-frequency measurements (0.001 Hz) were made with 90 minute waiting periods between points. Small magnetic field values were measured with a Hall probe.

Inelastic neutron scattering: Polycrystalline non deuterated $[Ni_{12}(O_2CMe)_{12}(chp)_{12}(H_2O)_6(thf)_6]\cdot 9\,THF$ (ca. 8 g) was sealed under helium in an aluminium cylindrical container of 15 mm diameter and 55 mm length. The experiments were carried out on the triple-axis spectrometer TASP at the SINQ neutron source (Paul-Scherrer Institute, Switzerland). Wavelength selection in the monochromator was achieved with the (002) reflection of pyrolytic graphite. In the analyser, a warm (room temperature) Beryllium filter and a pyrolytic graphite filter were used to fix the neutron final energy to 2.7 meV throughout the experiment. The axes of the spectrometer were chosen to scan the neutron energy loss region at several constant Q values. Scans were recorded at $T = 1.5$ and 15 K. The drawback of using a non-deuterated sample is that there is a large amount of incoherent scattering due to the hydrogen atoms. This leads to a smoothing of the Q dependence due to multiple scattering and a reduced overall intensity (large nuclear absorption).

  0947-6539/02/0821-4875 $ 20.00+.50/0

Acknowledgement

We thank the European Union for funding a TMR network on "Molecules as Nanomagnets" contract no. HPRN-CT-1999–00012. We also thank the EPSRC(UK) for funding for a diffractometer, a post-doctoral fellowship (to M.M.) and for a studentship (C.M.G.). The Swiss National Science Foundation, NFP47 program, also supported the work.

[1] a) R. Sessoli, H.-L. Tsai, A. R. Schake, S. Wang, J. B. Vincent, K. Folting, D. Gatteschi, G. Christou, D. N. Hendrickson, *J. Am. Chem. Soc*. **1993**, *115*, 1804–1816; b) R. Sessoli, D. Gatteschi, A. Caneschi, M. A. Novak, *Nature* **1993**, *365*, 141–142.

[2] a) J. Friedman, M. Sarachik, J. Tejada, R. Ziolo, *Phys. Rev. Lett.* **1996**, *76*, 3830–3833; b) L. Thomas, F. Lionti, R. Ballou, D. Gatteschi, R. Sessoli, B. Barbara, *Nature* **1996**, *383*, 145–146.

[3] C.Sangregorio, T. Ohm, C. Paulsen, R. Sessoli, D. Gatteschi, *Phys. Rev. Lett*. **1997**, *78*, 4645–4648.

[4] Z. Sun, C. M. Grant, S. L. Castro, D. N. Hendrickson, G. Christou, *Chem. Commun.* **1998**, 721–722.

[5] a) M. W. Wemple, D. M. Adams, K. S. Hagen, K. Folting, D. N. Hendrickson, G. Christou, *J. Chem. Soc. Chem. Commun.* **1995**, 1591–1593; b) E. K. Brechin, J. Yoo, M. Nakano, J. C. Huffman, D. N. Hendrickson, G. Christou, *Chem. Commun.* **1999**, 783–784.

[6] A. L. Barra, A. Caneschi, D. Gatteschi, D. P. Goldberg, R. Sessoli, *J. Solid State Chem.* **1999**, *145*, 484–487.

[7] A. L. Barra, A. Caneschi, A. Cornia, F. F. deBiani, D. Gatteschi, C. Sangregorio, R. Sessoli, L. Sorace, *J. Am. Chem. Soc.* **1999**, *121*, 5302–5310.

[8] C. Benelli, J. Cano, Y. Journaux, R. Sessoli, G. A. Solan, R. E. P. Winpenny, *Inorg. Chem.* **2001**, *40*, 188–189.

[9] J. C. Goodwin, R. Sessoli, D. Gatteschi, W. Wernsdorfer, A. K. Powell, S. L. Heath, *J. Chem. Soc. Dalton Trans.* **2000**, 1835–1840.

[10] A. L. Barra, D. Gatteschi, R. Sessoli, *Phys. Rev. B.* **1997**, *56*, 8192–8198.

[11] M. S. El Fallah, E. Rentschler, A. Caneschi, R. Sessoli, D. Gatteschi, *Inorg. Chem.* **1996**, *35*, 3723–3724.

[12] A. J. Blake, C. M. Grant, S. Parsons, J. M. Rawson, R. E. P. Winpenny, *J. Chem. Soc. Chem. Commun.* **1994**, 2363–4.

[13] Harris notation describes the binding mode as $[X.Y_1Y_2Y_3\ldots Y_n]$, in which X is the overall number of metals bound by the whole ligand, and each value of Y refers to the number of metal atoms attached to the different donor atoms. Therefore for both acetate and chp, there will be two values for Y. The ordering of Y is listed by the Cahn–Ingold–Prelog priority rules, hence O before N. See: R. A. Coxall, S. G. Harris, D. K. Henderson, S. Parsons, P. A. Tasker, R. E. P. Winpenny, *J. Chem. Soc. Dalton Trans.* **2000**, 2349–2356.

[14] C. Benelli, E. K. Brechin, S. J. Coles, A. Graham, S. G. Harris, S. Meier, A. Parkin, S. Parsons, A. M. Seddon, R. E. P. Winpenny, *Chem. Eur. J.* **2000**, *6*, 883–896.

[15] A. J. Blake, E. K. Brechin, A. Codron, R. O. Gould, C. M. Grant, S. Parsons, J. M. Rawson, R. E. P. Winpenny, *J. Chem. Soc. Chem. Commun.* **1995**, 1983–1984.

[16] G. L. Squires, *Introduction to the Theory of Thermal Neutron Scattering*, Cambridge University Press, Cambridge (UK), **1978**.

[17] E. K. Brechin, A. Graham, A. Parkin, S. Parsons, A. M. Seddon, R. E. P. Winpenny, *J. Chem. Soc. Dalton Trans.* **2000**, 3242–3251.

[18] I. M. Atkinson, C. Benelli, M. Murrie, S. Parsons, R. E. P. Winpenny, *Chem. Commun.* **1999**, 285–286.

[19] G. Kamieniarz, R. Matysiak, A. C. D'Auria, F. Esposito, C. Benelli, *Acta Phys. Pol. A* **2000**, *98*, 721–727.

[20] a) I. Mirebeau, M. Hennion, H. Casalta, H. Andres, H.-U. Güdel, A. V. Irodova, A. Caneschi, *Phys. Rev. Lett*. **1999**, *83*, 628–631; b) R. Caciuffo, G. Amoretti, A. Murani, R. Sessoli, A. Caneschi, D. Gatteschi, *Phys. Rev. Lett*. **1998**, *81*, 4744–4747; c) H. Andres, R. Basler, H.-U. Güdel, G. Aromi, G. Christou, H. Büttner, B. Rufflé, *J. Am. Chem. Soc*. **2000**, *122*, 12469–12477; d) J. M. Clemente, H. Andres, M. Aebersold, J. J. Borras-Almenar, E. Coronado, H.-U. Güdel, D. Kearley, H. Büttner, *J. Am. Chem. Soc*. **1999**, *121*, 10021–10027; e) H. Andres, J. M. Clemente, M. Aebersold, E. Coronado, H.-U. Güdel, D. Kearley, H. Büttner, *J. Am. Chem. Soc.* **1999**, *121*, 10028–10034.

[21] R. J. Birgenau, *J. Phys. Chem. Solids* **1972**, *33*, 59.

[22] J. J. Borràs-Almenar, J. M. Clemente-Juan, E. Coronado, B. S. Tsukerblat, *J. Comput. Chem*. **2001**, *22*, 985-.

[23] K. K. Nanda, L. K. Thompson, J. N. Bridson and K. Nag, *J. Chem. Soc. Chem. Commun.* **1992**, 1337–1338.

[24] M. A. Halcrow, J.-S. Sun, J. C. Huffman, G. Christou, *Inorg. Chem.* **1995**, *34*, 4167–4177.

[25] F. E. Mabbs, D. Collison, *Electron Paramagnetic Resonance of d Transition Metal Ions*, Elsevier, Amsterdam, **1992**, p. 1233.

[26] Using the mean field approximation, $E_{dip}/k = \mu_o(g\mu_B S)^2/4\pi Vk$, where V is the molar volume. For **1**: $g = 2.13$, $S = 12$ and $V = 4.7525 \times 10^{-27}$ m^3; therefore $E_{dip}/k = 0.086$ K.

[27] W. Wernsdorfer, N. Aliaga-Alcalde, D. N. Hendrickson, G. Christou, *Nature* **2002**, *416*, 406–409.

[28] V. Villar, PhD thesis, Université Joseph-Fourier, Grenoble (France), **2001**.

[29] J. Cosier, A. M. Glazer, *J. Appl. Crystallogr.* **1986**, *19*, 105–107.

[30] W. Clegg, *Acta Crystallogr. Sect. A* **1981**, *37*, 22–28.

[31] P. T. Beurskens, G. Beurskens, W. P. Bosman, R. de Gelder, S. Garcia-Granda, R. O. Gould, R. Israel, J. M. M. Smits, DIRDIF-96 program system, University Crystallography Laboratory, University of Nijmegen (The Netherlands), **1996**.

[32] G. M. Sheldrick, SHELXL-93, program for crystal structure refinement, University of Göttingen, Göttingen (Germany), **1993**.

Received: March 25, 2002 [F3972]

